Journal of
Materials Chemistry A

Solvent-free Vacuum Growth of Oriented HKUST-1 Thin Films

Journal:	*Journal of Materials Chemistry A*
Manuscript ID	TA-ART-05-2019-005179.R2
Article Type:	Paper
Date Submitted by the Author:	01-Aug-2019
Complete List of Authors:	Han, Sungmin; University of Texas at Austin, Department of Chemistry Ciufo, Ryan; University of Texas at Austin, Department of Chemistry Meyerson, Melissa; University of Texas at Austin, Chemistry Keitz, Benjamin; University of Texas at Austin, Department of Chemical Engineering Mullins, Charles; University of Texas at Austin, Department of Chemical Engineering

SCHOLARONE™
Manuscripts

ARTICLE

Solvent-free Vacuum Growth of Oriented HKUST-1 Thin Films

Sungmin Han,[a] Ryan A. Ciufo,[a] Melissa L. Meyerson,[a] Benjamin K. Keitz,[b] C. Buddie Mullins[a,b,c]*

Received 00th January 20xx,
Accepted 00th January 20xx

DOI: 10.1039/x0xx00000x

Thin films of ultrahigh porous metal organic frameworks (MOFs) are highly desirable because the unique characteristics of MOFs could then be incorporated into micro-electronic devices, sensors, and membranes. Here we report a new thin film growth method for highly oriented $Cu_3(BTC)_2$ (HKUST-1) under vacuum without the use of solvents. Using layer-by-layer (LBL) growth, we sequentially deposited H_3BTC from a chemical vapor deposition process and Cu from a physical vapor deposition process. Adopting this methodology, we grew thin films of HKUST-1 by sequentially depositing one monolayer (ML) of Cu after each H_3BTC deposition cycle. The transition of Cu^0 to Cu^{2+} by forming paddle-wheel units of HKUST-1 was confirmed by XPS, and is facilitated by background gas molecules, O_2 and H_2O, with no indication of copper oxide formation. Our HKUST-1 thin films have two distinct planes, the (220) plane detected by glancing angle XRD and the (222) plane identified by in-plane XRD, which indicates that the HKUST-1 thin films are highly oriented. Moreover, the thickness of the HKUST-1 thin films linearly increased with the number of LBL cycles by ~ 20 nm for each LBL cycle as measured by AFM. Finally, we measured H_2O desorption in a 100nm HKUST-1 film and observed the existence of strongly bound H_2O molecules absorbed within the HKUST-1 film, which predominantly desorb at ~398 K. Overall, we show how to control the growth of highly oriented HKUST-1 thin films through a bottom-up approach by directly depositing H_3BTC and Cu under high vacuum.

1. Introduction

Metal-organic frameworks (MOFs) are a new class of microporous materials, which consist of metal containing inorganic nodes and organic linkers.[1,2] Because of their ultrahigh porosity and tunability, they have been widely applied in gas storage,[3–9] CO_2 capture,[10–14] hydrocarbon separation,[15–21] catalysis,[22–24] and as microporous magnets[25–29]. In addition to these applications, the growth of MOF thin films has received significant attention because it could facilitate the direct fabrication of MOFs into microelectronic devices, such as gas sensors,[30–32] electronic & opto-electronic devices,[33–35] and also drug delivery[36,37]. MOF thin films can be also applied to microporous membranes for gas separations.[38–40] The majority of MOF thin film deposition methods that have been developed thus far have been adapted from powder-type MOF preparation methods using various solvents. In particular it has been reported that solvent based MOF thin film growth methods can be widely applied in the field of gas sensors by directly fabricating the MOF on the surface of electrodes and other supports.[29,41–45] However the solvent based MOF growth methods have limits regarding direct applications in the semiconductor micro-chip fabrication process which is typically conducted under vacuum. Primarily because the aqueous solvents can contaminate the vacuum chambers and also corrode the fabrication system. Furthermore, the used solvents become environmentally harmful chemical wastes, involving additional costs for their safe disposal.

To overcome these disadvantages, vapor-based methods for growing MOF films are required. Stassen *et al*. has recently reported a solid-vapor based ZIF-8 thin film growth method using chemical vapor deposition (CVD) of 2-methylimidazole (HmIm).[46,47] In this study, the ZnO layers grown by an atomic layer deposition (ALD) technique were exposed to HmIm vapor for the transformation of ZnO to ZIF-8 on the basis of a neutralization reaction (ZnO + HmIm ➔ ZIF-8 + H_2O). They showed that patterned ZIF-8 films could be prepared employing patterned ZnO layers. An analogous ZIF-8 growth method was used to grow gas separation membranes by converting ZnO layers to ZIF-8 on permeable Al_2O_3 substrates.[40] Because these techniques for ZIF-8 film growth involve the conversion of ZnO precursor layers to the ZIF-8 structure, which is a top-down approach, they are susceptible to self-inhibition when thick ZnO layers are used. Specifically, in both studies,[40,46] the authors found that the continuous diffusion of HmIm to the bottom ZIF-8 - ZnO interface is slower and limited by initially converted ZIF-8 layers, which are on the top of the ZnO layers. These studies highlight the need for improved methods to control MOF thin film synthesis.

HKUST-1, $[Cu_3(BTC)_2]$ (BTC: Benzene-1,3,5,-tricarboxylic acid), is one of several commercialized MOFs and is widely studied because of its coordinately unsaturated open metal sites.[48,49] The open metal sites in HKUST-1 function as chemically active centers, and thus, HKUST-1 has shown various interesting applications such as selective gas adsorption and separation,[50–

a. Department of Chemistry, University of Texas at Austin, Austin, Texas 78712-0231, United States.
b. McKetta Department of Chemical Engineering, University of Texas at Austin, Austin, Texas 78712-0231, United States.
c. Center for Nano and Molecular Science and Technology, Texas Materials Institute, Center for Electrochemistry, University of Texas at Austin, Austin, Texas 78712-0231, United States. E-mail: mullins@che.utexas.edu
†Electronic Supplementary Information (ESI) available. *See DOI: 10.1039/x0xx00000x*

[54] Lewis acid catalysis,[55] and proton transfer channels.[56] Thin films of HKUST-1 have also been widely investigated primarily regarding highly-oriented growth using self-assembled organic monolayers (SAMs).[57,58] The SAMs are famous for their relatively easy preparation and can be patterned using facile micro contact printing. Thus, employing the SAMs can allow the synthesis of surface bound thin film SURMOFs (SURfaceMOFs) which are homogeneous and atomically flat. Specifically, the -COOH or -OH or -CH_3 terminated SAMs, which are the main functional groups in the organic linker for HKUST-1 (H_3BTC), can promote the successful growth of 2D thin film HKUST-1 via immersing SAM coated films in the metal ion (e.g., Cu^{2+} or Zn^{2+}) and the ligand (BTC) containing solutions sequentially.[57,58] This SAM based method leads to the growth of highly-oriented HKUST-1 films (the -COOH for the {200} planes and the -OH for the {222} planes). HKUST-1 MOF thin films can also be directly grown on basic metal oxide interfaces (e.g., Al_2O_3) without SAMs,[59] and the overall growth can be controlled using UV irradiation.[60] Similar to the case of ZnO, copper oxides and copper hydroxides can be precursors for HKUST-1 thin film growth on various substrates.[59,61,62] Although SAMs and other oxide interfaces provide growth sites for the deposition of HKUST-1 thin films, they are still solution-based methods basically following the HKUST-1 powder preparation method.

As a new approach, we report the physical vapor deposition (PVD) of Cu^0 and the chemical vapor deposition (CVD) of H_3BTC on a SiO_2/Si(100) substrate for the solvent-free growth of HKUST-1 thin films (~20-200 nm in thickness) in a high vacuum chamber (base pressure 2.0 x 10^{-8} Torr), which is also expected to be applicable in the microelectronic fabrication process. (See Scheme 1). Similar to the suggested growth concept in this study, the combined method of PVD of metal atoms and CVD of organic ligands has been applied to forming "so-called" 2D-metal organic networks on various metal surfaces previously (typically one layer in thickness).[63–65] Improving this 2D based method, the layer-by-layer (LBL) growth concept was adopted in this study as a way of achieving bottom-up thin film growth. Our successfully grown HKUST-1 thin films have polycrystalline features, but they are preferentially grown and show the (220) and (222) planes as their primary planes measured from glancing angle XRD and in-plane XRD respectively. We have further analyzed our HKUST-1 thin films using XPS and AFM and also successfully measured the adsorption and desorption of H_2O on our HKUST-1 thin films under high vacuum. Overall, we suggest a new growth method of highly oriented HKUST-1 thin films by controlling the depositions of H_3BTC and Cu under high vacuum.

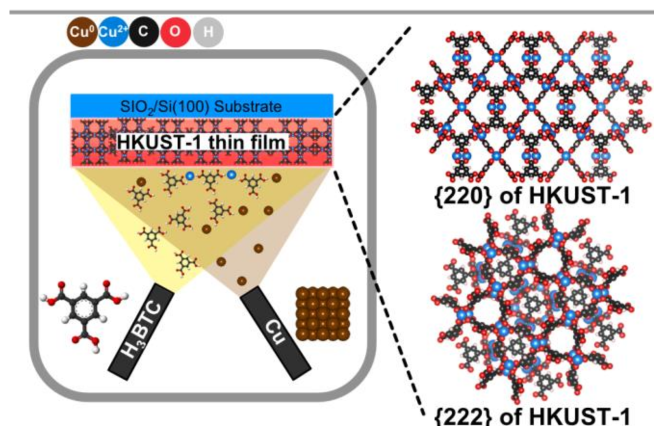

Scheme 1. Schematic description of HKUST-1 thin film growth in the high vacuum chamber

2. Experimental Section

HKUST-1 thin films were grown in a high vacuum system with a base pressure of ~2.0 x 10^{-8} Torr. Our high vacuum system consists of two different parts. One part is a sample growth chamber equipped with an e-beam evaporator for the PVD of Cu and a thermal evaporator for the CVD of H_3BTC. The other part is a sample loading and thermal analysis chamber equipped with a quadrupole mass spectrometer (QMS). We used a SiO_2/Si(100) wafer from MTI as a substrate for the growth of HKUST-1 thin films, where 300 nm SiO_2 layers were grown on a Si(100) substrate. A piece of the SiO_2/Si(100) wafer, which has the dimensions 0.9 cm x 0.9 cm x 0.5mm, was loaded on to a sample holder composed of a tantalum plate located in the sample loading chamber. The sample holder is mounted to two tantalum wires which can resistively heat the loaded sample and also provide a thermal contact between the sample and a liquid nitrogen bath for cooling. The sample temperature was measured by a K-type thermocouple spot-welded to the top edge of the tantalum plate.

As mentioned earlier, we used an e-beam evaporator for the PVD of Cu. The electrons from a tungsten filament were directed (via biasing) to metallic Cu pellets filled in a molybdenum (Mo) crucible. The Cu deposition rate was held at 0.05 Å/s, as calibrated by a quartz crystal microbalance (QCM) and its controller (Inficon SQM-160) assuming the thickness of 1 ML (monolayer) Cu to be 2.56 Å. To perform the CVD of H_3BTC, 95% H_3BTC powders (from Sigma Aldrich) were placed in a Al_2O_3 crucible and resistively heated while also monitoring its temperature by a K-type thermocouple. The H_3BTC temperature was fixed at 473 K (200 °C) during the deposition process. Using manual shutters in front of both the Cu and H_3BTC evaporators, it was possible to control the deposition time of each evaporator. Before the beginning of the HKUST-1 thin film growth, the sample growth chamber was back-filled with H_2O (2.5 x 10^{-5} Torr) and O_2 (2.5 x 10^{-5} Torr), which increased the chamber pressure to 5.0 x 10^{-5} Torr. 4 ML Cu were initially deposited on the SiO_2/Si(100) wafer sample, and then H_3BTC and Cu were exposed sequentially. The sample was held at 323 K during the deposition of Cu and H_3BTC, followed by annealing at 343 K for 15 minutes after completion of the deposition process while maintaining the back-filled H_2O and O_2 in the chamber at 5.0 x 10^{-5} Torr. Successfully grown HKUST-1 thin film samples were further characterized by ex-situ analysis using X-ray diffraction (XRD), X-ray photoelectron spectroscopy (XPS), and atomic force microscopy (AFM). To minimize complications due to the SiO_2/Si(100) substrate during XRD analysis, we adopted two different XRD techniques with Cu K_α radiation in the Rigaku Ultima IV; glancing-angle XRD (GAXRD) and in-plane XRD (IPXRD), which allow us to observe the

 This journal is © The Royal Society of Chemistry 20xx

Please do not adjust margins

crystallinity of the HKUST-1 thin films. The GAXRD was conducted with a scan rate of 0.5°/min in 0.02° steps, and the IPXRD was operated with a scan rate of 0.1°/min in 0.02° steps. Surface chemical states and bonds were identified by a Kratos Axis Ultra XPS system using a monochromatic Al-K_{α} X-ray source (1486.6 eV), and the spectra were calibrated by the C1s peak at 284.6 eV as a standard. Casa XPS analysis software was used to conduct peak deconvolution of measured XPS spectra adopting a Shirley background and line shapes with a combination of the Gaussian and Lorentzian functions, which keeps the full-width at half maximum (FWHM) of deconvoluted peaks in all XPS spectra lower than 2.5 eV. The thickness and roughness of the HKUST-1 thin films were characterized by a non-contact atomic force microscope (XE-100). We also measured H_2O adsorption and desorption capability of the HKUST-1 thin films employing temperature programmed desorption (TPD). To conduct the TPD experiments, we first activated the HKUST-1 thin film sample by heating it from 298 K to 398 K at a temperature ramp rate of 0.5 K/s and then holding it at 398 K for 20 minutes, at which time there was no longer any further H_2O desorption as detected by the QMS. The activated HKUST-1 thin film was then cooled to 120 K and exposed to back-filled H_2O molecules at 2.0 x 10^{-6} Torr for 30 minutes. After that, the H_2O exposed HKUST-1 thin film was heated from 120 K to 398 K at a rate of 0.5 K/s and held at 398 K for 20 minutes to complete the H_2O desorption. During this process, a m/z^+ =18 signal was recorded by the QMS (Extorr xt100m). We did not increase the HKUST-1 sample temperature above 398 K in order to prevent the decomposition of the deposited HKUST-1 structures.

3. Results and discussion

As shown in Scheme 1, the CVD of H_3BTC and the PVD of Cu are performed to grow the HKUST-1 thin film on a SiO_2/Si(100) substrate under vacuum. Oxidized Cu precursor layers (e.g., Cu_xO_y, $Cu(OH)_2$)[59,61,62] were not required to grow the HKUST-1 film. Adopting a bottom-up growth concept, H_3BTC and Cu were directly exposed to the substrate sequentially establishing a layer-by-layer (LBL) growth protocol. At the beginning of the growth, 4 ML of Cu (~ 1 nm thick) was deposited directly on the SiO_2//Si(100) substrate. This initial Cu layer was mainly used as a substrate upon which H_3BTC molecules in the first deposition cycle can be organized. It is known that H_3BTC molecules can form porous supramolecular structures not only by themselves but also on various surfaces, such as Cu, Ag, Au and graphite.[66–74] We were inspired by these studies to use the supramolecular structures of H_3BTC as templates to grow the HKUST-1 thin films.

We found the optimized growth conditions to consist of an exposure time of H_3BTC of 3 minutes in each cycle while holding the evaporation temperature of H_3BTC at 473 K (200 °C). The vacuum chamber was back-filled with H_2O and O_2 to a total pressure of 5.0 x 10^{-5} Torr. During the growth, the sample was held at 323 K, which was followed by annealing at 343 K for 15 minutes all with 5.0 X 10^{-5} Torr of H_2O and O_2. As shown in Figure 1, we optimized the amount of Cu in each cycle using a 5 LBL cycled HKUST-1 thin film as a representative case by measuring

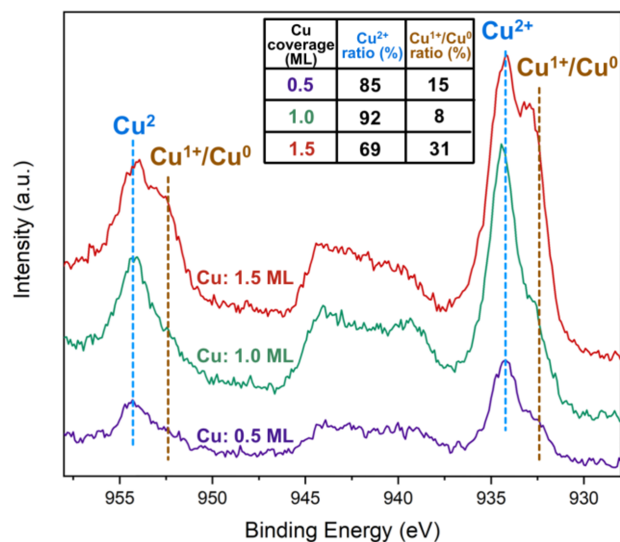

Figure 1. XPS analysis for the Cu2p region of 5 LBL cycles of HKUST-1 thin films. To optimize the amount of Cu in each layer, the 5 cycled HKUST-1 thin films were grown by using 0.5 ML Cu (purple), 1.0 ML Cu (green), and 1.5 ML Cu (red) in each LBL cycle. We highlighted the main peak for Cu^{2+} (~ 934 eV) and its sub peak with light-blue and the Cu^{1+}/Cu^0 peak (~ 932 eV) and its sub peak with brown.

the oxidation state of Cu via XPS, which is a widely used analysis method for confirming the Cu^{2+} state in HKUST-1.[34,75–82] Specifically, a 1 ML Cu deposition in each cycle for the 5 cycled film shows the highest ratio of Cu^{2+} to Cu^{1+}(or Cu^0), 92 % and 8 % respectively by integrating the deconvoluted peak area of Cu^{2+} (~ 934 eV, light-blue line) and Cu^{1+}/Cu^0 (~ 932 eV, brown line), which also has clear satellite peaks by Cu^{2+} from 936 eV – 946 eV. This Cu^{2+} to Cu^{1+}/Cu^0 ratio is similar to previously reported values from the HKUST-1 powders and thin films.[81,82] When we decreased the amount of Cu to 0.5 ML, the Cu^{2+} peak intensity is about a half of the 1.0 ML case, which indicates that 0.5 ML Cu does not fully saturate the H_3BTC layers. However, a deposition of 1.5 ML Cu in each cycle causes over-saturation of the H_3BTC layers, as it shows a higher intensity of the Cu^{1+}/Cu^0 ratio with almost the same intensity of Cu^{2+} compared to the 1.0 ML Cu case. This result indicates that the extra Cu atoms are partially oxidized or remain unreacted. Based on these results, we fixed the deposition amount of Cu in each cycle at 1 ML. There was no indication of copper oxide formation in any of the tests since their O1s XPS spectra do not show any components in the range of 530.5 eV - 529.5 eV as shown in Figure S1, which is a typical range for the O1s feature from Cu_2O and CuO.[76,83,84]

As mentioned above, Cu and H_3BTC deposited samples were annealed at 343 K for 15 mins to complete the HKUST-1 film growth. After finishing growth, we measured the crystallinity of our samples using glancing-angle XRD (GAXRD). GAXRD is a widely adopted asymmetric out-of-plane XRD technique, which can analyze variously oriented planes in thin films with less interruption from their supporting substrates and the techniques have also been adopted for HKUST-1 thin film analysis previously.[33,34,85–87] Our HKUST-1 thin films displayed peaks at ~ 9.2° and ~ 18.5° in the GAXRD (gray line in Figure 2a), which corresponds to the (220) and (440) planes of HKUST-1 respectively. (We will further discuss its crystallinity in the following section.) The unannealed 5 cycles of H_3BTC (blue line

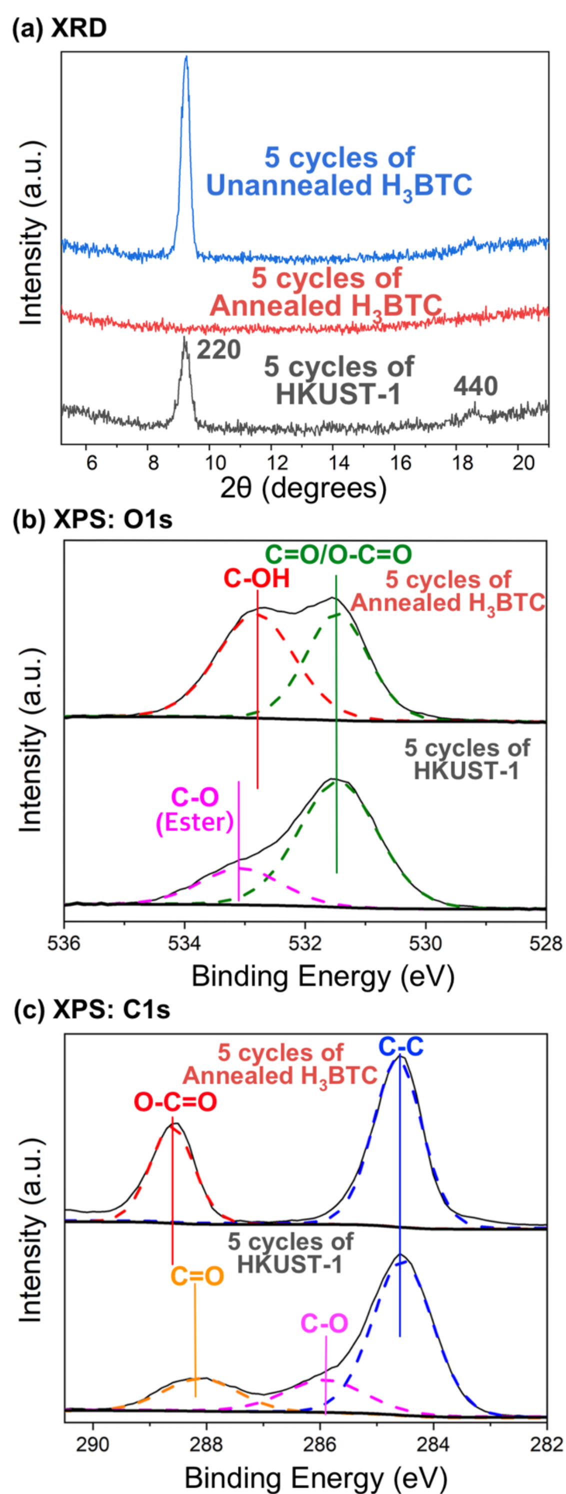

Figure 2. (a) XRD patterns for the 5 cycles of unannealed H_3BTC (blue, 5 times of H_3BTC deposition for 3 minutes in each), the 5 cycles of HKUST-1 films (gray), and the 5 cycles of annealed H_3BTC at 343 K for 15 mins (red). (b) and (c) show the XPS spectra of O1s and C1s regions respectively for the 5 cycles of annealed H_3BTC and the 5 cycles of HKUST-1 film.

in Figure 2a, five consecutive rounds of H_3BTC deposition on the substrate for 3 mins each, 15 mins in total), which is directly grown on the initial Cu layer without including Cu deposition between each H_3BTC deposition, shows very similar XRD patterns compared to the HKUST-1 thin films even though there are still some differences between these two XRD patterns above 25° in 2θ as shown in Figure S2. The unannealed 5 cycled H_3BTC fully covers the top surface of the substrate, which shows a different color compared to a blank SiO_2/Si(100) substrate. (Figure S3) Moreover we did not detect Cu features in the Cu2p region in its XPS spectrum in Figure S2b, which would appear if the H_3BTC molecules did not fully cover the 4 ML Cu deposited SiO_2/Si(100) substrate. This means there are multilayers of H_3BTC forming 3D structures by themselves. From the XRD results, we propose that the deposited H_3BTC molecules are long-range ordered on the initial Cu layer (~ 1 nm of thickness) on the SiO_2/Si(100) substrate to form the supramolecular structures based on hydrogen bonds (H-bonds) which leads to the HKUST-1 like structures. Similar to this study, it has been found that the Cu layer on the Au(111) surface provides binding and regular organization sites for H_3BTC molecules without changing the oxidation state of the Cu atoms.[88]

Since the H_3BTC molecules are connected to each other only by H-bonds, they lose their crystallinity after annealing at 343 K for 15 mins (red line in Figure 2a), likely being converted into randomly ordered H-bonded clusters. Even though the 5 cycles of H_3BTC were annealed at 343 K, it is not a high enough temperature to cause the desorption of multilayers of H_3BTC, which needs to be heated to ~ 573 K as previously found.[89] There is also no color change between the unannealed and annealed films as shown in Figure S3, and it was possible to detect the H_3BTC molecules on the annealed surface by O1s and C1s XPS measurements (which will be discussed in the following section). The lack of crystallinity in the annealed 5 cycled H_3BTC sample (see Figure 2a) supports the notion that Cu atoms in the initial 4 ML Cu layer do not broadly diffuse into the H_3BTC layers to form a HKUST-1 structure and also there is no trace of Cu in the Cu2p region in XPS as described in Figure S2b. This lack of crystallinity is very interesting since an HKUST-1 structure can be annealed to 343 K and retain its crystallinity after annealing. As we mentioned above, the XRD patterns of the 5 cycled HKUST-1 are similar to the unannealed 5 cycled H_3BTC. Both cases have a main peak at ~ 9.2° of 2θ. The full-width half maximum (FWHM) of this peak in the unannealed 5 cycled H_3BTC is ~ 0.3°, which is slightly smaller than the FWHM of the same peak in the 5 cycled HKUST-1 (~ 0.37°) indicating the decrease of average grain sizes. Relatedly, deposited Cu atoms in each cycle react with H_3BTC molecules, which shrinks the structure by forming coordinate bonds between Cu and H_3BTC, which leads to the FWHM of the HKUST-1 film at ~ 9.2° being increased. We can also see that the unannealed 5 cycled H_3BTC have a stronger peak at ~ 9.2° than the corresponding peak on the HKUST-1 film, but its peak at 18.5° is weaker than the one on the HKUST-1 film related to the (440) plane of HKUST-1. These results indicate that the crystal structures of the HKUST-1 thin film are originating from the 3D supramolecular structures of H_3BTC, but there are still some structural changes caused by the 1.0 ML Cu deposition after each H_3BTC deposition. Furthermore, it has been found that H_3BTC molecules can be densely packed and regularly organized on Cu surfaces by forming chain structures composed of up-right oriented H_3BTC molecules anchored on Cu atoms, and then

This journal is © The Royal Society of Chemistry 20xx

Please do not adjust margins

extra H_3BTC molecules form 3D structures based on hydrogen bonds (H-bonds) with each other.[89,90]

We also compared differences in O1s and C1s XPS spectra of the annealed 5 cycles of H_3BTC (the same growth conditions as the HKUST-1 thin film except with no Cu deposition between H_3BTC cycles) and the 5 cycled HKUST-1 thin film in order to prove that the deposited Cu atoms interact with the H_3BTC structure. The O1s spectrum of the annealed 5 cycles of H_3BTC shows two peaks having similar intensities at 531.5 eV for C=O/O-C=O bonds by carboxyl groups and its split peak at 532.8 eV for C-OH bonds,[79,91–93] which is similar to previously observed H-bonded H_3BTC molecules on a Ag coated Au(111) surface and a Cu(100) surface.[72,89] However, the 5 cycled HKUST-1 films has a peak at 533.1 eV for C-O bonds (ester type oxygen) and the other peak is at 531.5 eV for C=O/O-C=O bonds (carboxylate type oxygen).[79,91–93] Consistent with previous HKUST-1 studies,[80,91,92] the C-O bond peak shows lower intensity than the C=O/O-C=O bond peak. This ester type C-O bond can be formed when the H_3BTC is deprotonated and forms coordinate bonds with Cu^{2+}, Cu-O-C. These results also confirm that H_3BTC molecules in the annealed 5 cycled H_3BTC are not fully deprotonated to make new covalent bonded clusters by forming ester type C-O bonds with each other, but they still exist as H-bonded clusters. The C1s XPS spectra of H_3BTC and HKUST-1 also shows clear differences depending on their chemical status (see Figure 2c). The annealed 5 cycles of H_3BTC mainly shows C-C sp2 bonds at 284.6 eV[75,91,94,95] and also has a peak for O-C=O(~ 288.7 eV) bonds from the carboxyl group of H_3BTC[91,94,96,97]. When we compare these results to the 5 cycled HKUST-1 thin film, the HKUST-1 sample has a peak at 284.6 eV for C-C bonds and shows the formation of C-O bonds at ~ 285.9 eV by the ester type bond formation with Cu^{2+} ions (Cu-O-C) as previously observed,[91,94,95] which also has been detected in the O1s spectrum. Furthermore, there is a peak at 288.3 eV indicating C=O bonds,[91,94,97] which is 0.4 eV lower than the peak of carboxyl groups (O-C=O) observed in the annealed H_3BTC sample, so it also supports the deprotonation of H_3BTC to form the Cu-O-C bond in HKUST-1.

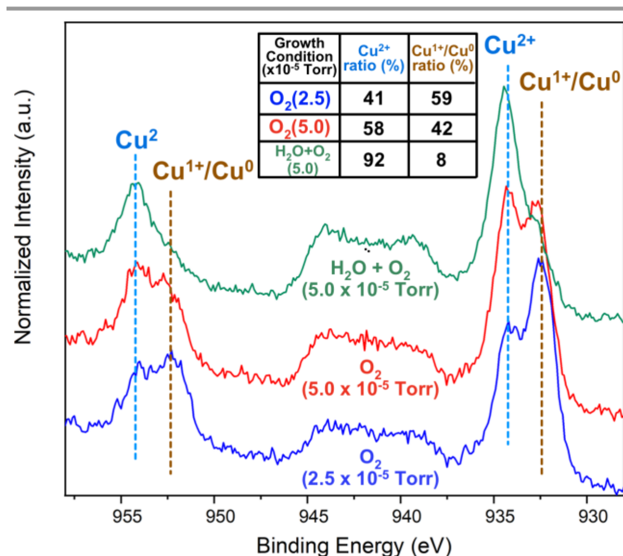

Figure 3. XPS analysis for the Cu2p region of 5 LBL cycles (1 ML Cu deposited in each cycle) of HKUST-1 thin films grown with H_2O + O_2 background gases at total pressure of 5.0 x 10^{-5} Torr (2.5 x 10^{-5} Torr in each), pure O_2 at 5.0 x 10^{-5} Torr, and pure O_2 at 2.5 x 10^{-5} Torr. We highlighted the main peak for Cu^{2+} (~ 934 eV) and its satellite peak (~ 954 eV) with light-blue and the main Cu^{1+}/Cu^0 peak (~ 932 eV) and its satellite peak (~ 952 eV) with brown.

As we explained above, we directly deposited Cu^0 atoms on the H_3BTC covered surface instead of using other Cu based solid precursors, such as CuO and $Cu(OH)_2$, which have been used in previous studies.[59,61,62] However, we adopted O_2 as a background gas expecting it to work as the ionization agent of Cu and the deprotonation agent of H_3BTC. Furthermore, it has been found that water vapor enhances the solid state conversion of ZnO to ZIF-8.[46] To investigate the synergistic effect of the background gases, H_2O and O_2, we grew HKUST-1 films under two different pure O_2 back-filled conditions (2.5 x 10^{-5} Torr and 5.0 x 10^{-5} Torr) and compared them to the sample grown under a H_2O and O_2 mixed condition (total pressure: 5.0 x 10^{-5} Torr, H_2O (2.5 x 10^{-5} Torr) + O_2 (2.5 x 10^{-5} Torr)). Since the formation of copper oxide has not been found in XPS in any of our tests (see Figure S1 and S4), we assumed that the oxidation of Cu^0 to Cu^{2+} is caused by the formation of the paddle-wheel units of HKUST-1, which consist of BTC^{3-} (deprotonated H_3BTC) and Cu^{2+}. As shown in Figure 3, it is possible to detect Cu^{2+} in XPS even by back-filling the chamber with the pure O_2. However, there are differences in the ratio of Cu^{2+} to Cu^{1+}(or Cu^0) depending on the applied pressure of O_2. When the O_2 pressure is increased from 2.5 x 10^{-5} to 5.0 x 10^{-5}, there is more Cu^{2+} formation, which means the O_2 molecules are involved in the oxidation of the Cu atoms. There is still no indication of any Cu oxides based on the O1s XPS in each case (Figure S4), so the O_2 molecules mainly work to ionize Cu and deprotonate H_3BTC. The H_2O and O_2 mixed case showed the highest ratio of Cu^{2+} compared to others. This phenomenon can be caused by the solvation effect of water, for which it has been thermodynamically proven that the coordinated H_2O molecules stabilize the paddle-wheel units of the HKUST-1.[98–100] In particular, it is also known that the deprotonation of ligands is essential in the growth of various MOFs,[101] so we suspect that the background H_2O molecules facilitate the deprotonation of H_3BTC, which allows more facile oxidation of Cu^0 to Cu^{2+}.

We also grew 2, 5, and 10 cycled samples to check their crystallinity by adopting two different XRD techniques, the glancing-angle XRD (GAXRD) and the in-plane XRD (IPXRD) as shown in Figure 4a and 4b respectively. These samples are uniformly coated on the substrates and highly reflective, like a mirror, which show different color depending on the number of growth cycles as indicated in Figure S5. In overall XRD measurements, the (220) plane at 9.2° in 2θ shows the strongest intensity in the GAXRD (Figure 4a), and the (222) plane at 10.8° in 2θ is a dominant plane in the IPXRD (Figure 4b), which means our HKUST-1 thin films are highly oriented.[33,34,48,102] However, additional peaks for HKUST-1 above 20° appear as indicated in Figure S6, which are due to the polycrystalline properties of our HKUST-1 thin films. The XRD peaks in both measurements are slightly shifted towards lower angles compared with HKUST-1 simulated peaks[48] It has been found that the top surface compositions of the substrate

This journal is © The Royal Society of Chemistry 20xx

Please do not adjust margins

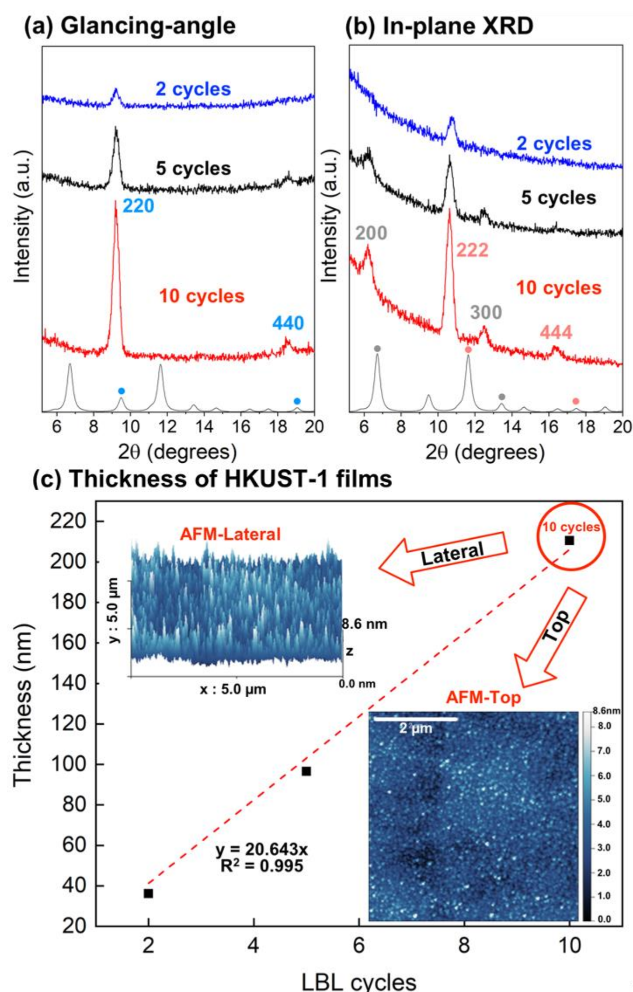

Figure 4. (a) the glancing-angle and (b) the in-plane XRD measurements for 2, 5, 10 LBL cycles of HKUST-1 thin films with simulated HKUST-1 XRD patterns (black lines at the bottom of each figure). (c) shows the thickness of these HKUST-1 thin films measured by AFM. Top and lateral views of the 10 cycled HKUST-1 film are also included as insets.

directly affect the thin film structures grown on it.[103] Thus, we suspect that the XRD peak shifts could be related to the alignment of H_3BTC molecules on the Cu covered SiO_2/Si(100) substrate since we have already found that the HKUST-1 structure is derived from the deposited H_3BTC layers as shown in Figure 2. Moreover, there would be some accumulated strains within the H_3BTC-Cu-SiO_2/Si(100) structures, which possibly affects the HKUST-1 thin film structures.[103–105] Specifically in the GAXRD measurements, the peak intensity for the (220) plane at 9.2° continuously gets bigger with increasing number of LBL cycles, but the FWHM of this peak stays almost the same, ~ 0.37°, in all tested HKUST-1 films. The (440) plane is also observed at ~ 18.5°, which is a sub-plane of (220). However, our samples do not show other main planes for HKUST-1, such as peaks at ~ 6.5° for the (220) plane and ~ 11.5° for the (222) plane. For the IPXRD, the peak for the (220) plane located between 9° and 10° is not observed, but all the samples have a peak at 10.8°, which is close to the (222) plane of HKUST-1. As with the (220) peak in the GAXRD, the thicker the sample is, the more intense the peak for the (222) plane, with a similar FWHM value (~ 0.36°). From the 5 cycled samples, XRD peaks for the (200) and (300) planes are also observed at ~6.5° and ~ 13° respectively, and they also get larger on the 10 cycled sample. Although the (222) plane is detected as a main plane in the IPXRD measurement, which shows our HKUST-1 thin films are highly oriented, the observation of the (200) plane on thicker films indicates a polycrystalline character for our samples. The two dominant planes in our measurements, (220) and (222), have also been observed in a previous study in which octahedral shaped HKUST-1 particles grown along the <100> direction are well organized on a gold substrate.[102]

After analyzing the structural properties of our HKUST-1 thin films, we investigated their thickness and surface characteristics using atomic force microscopy (AFM). As shown in Figure 4c, the thickness of our 2, 5, and 10 cycled HKUST-1 thin films are analyzed. (more detailed results are in Figure S7) To conduct these measurements, we masked some portions of the substrates and then grew the HKUST-1 films. With more LBL cycles, the thickness of our samples linearly increases, as expected, with a R^2 value of 0.99. Specifically, the 2, 5, and 10 cycled samples have average thicknesses of 37.5, 97, and 210 nm respectively, where each LBL cycle deposits a ~ 20 nm-thick HKUST-1 film. The root mean square (RMS) roughness also increases depending on the number of LBL cycles as with other MOF thin film growth studies,[106] but our samples are quite flat since even the 200 nm thick sample (10 cycles) has ~ 1 nm for the RMS roughness. This can be observed from the top view and lateral view of the 10 cycled HKUST-1 film in the inset to Figure 4c. The top view shows its continuous and homogeneous top surface. In the lateral view, it is interesting to see that the densely packed nano rods on the surface are regularly organized in an up-right orientation. These AFM observations are further evidence for the highly-oriented structure of our HKUST-1 thin films.

It is known that the HKUST-1 is an exceptional H_2O sensor, which tends to be adsorbed at the 9 Å main cages of HKUST-1.[32,107–109] Although the adsorption energy of H_2O is known to be 48 - 55 kJ/mol,[110–113] previous H_2O isotherm measurements have shown hysteresis during the H_2O desorption process,[114,115] which indicates some water molecules are strongly chemisorbed in the HKUST-1 structure. These strongly chemisorbed H_2O molecules can be removed by an activation process, which typically involves holding the HKUST-1 structure at ~ 120 °C under vacuum.[60,112,115] Furthermore it has been found that the weight of HKUST-1 powders rapidly decreases from the evaporation of strongly bound H_2O and other solvent molecules when the temperature increases from 25 °C to 150 °C in previous TGA analysis.[78,116] In our study, we also tested the adsorption and desorption of H_2O in order to measure the porosity and gas uptake properties of our HKUST-1 thin films. To conduct this experiment, the activated 5 cycled HKUST-1 thin film was exposed to back-filled H_2O molecules (2.0×10^{-6} Torr). This is a constant pressure H_2O adsorption experiment at a significantly lower pressure compared to previous isotherm tests using HKUST-1 powders in which the vapor pressures of H_2O were varied up to its saturated vapor pressure (~23 Torr) at room temperature.[110–115] We first tested the adsorption of H_2O while the sample was held at 120 K for 30 mins. Shown in Figure

This journal is © The Royal Society of Chemistry 20xx

Please do not adjust margins

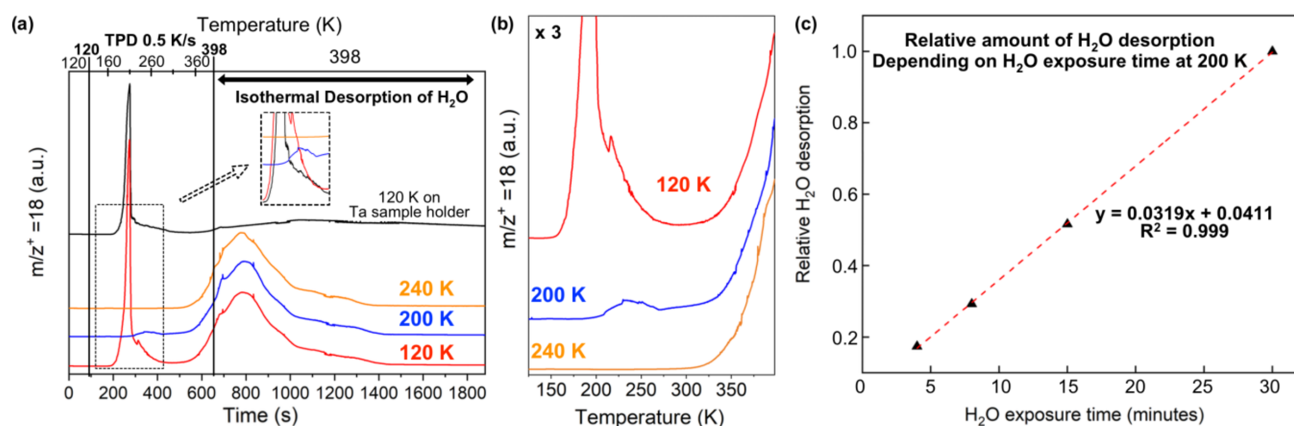

Figure 5. (a) The desorption spectra of H_2O molecules exposed to the 5 cycled HKUST-1 thin film at 120 K (red), 200 K (blue), and 240 K (orange) for 30 mins at 2 x 10^{-6} Torr H_2O for each. As a reference, we also added the desorption spectrum of H_2O exposed to the sample holder (made of tantalum) at 120 K for 30 mins at 2 x 10^{-6} Torr H_2O (black). After the H_2O adsorption at different temperatures, the samples were held at 120 K for 2 mins and then heated to 398 K at 0.5 K/s to conduct temperature programmed desorption (TPD). The inset describes a 5 times magnified temperature range of 130 K to 300 K. When the samples reached at 398 K, they were kept at 398 K for 20 mins for the isothermal H_2O desorption. (b) Zoomed out H_2O desorption spectra. (c) Relative amount of H_2O desorption by different H_2O exposure times at 200 K. (30, 15, 8, and 4 mins)

5a are the results of temperature programmed desorption (TPD) measurements. Our measurement protocol is similar to that used extensively in surface science experiments performed under ultrahigh vacuum conditions. Here we measured the desorption of H_2O by heating the sample from 120 K to 398 K at a rate of 0.5 K/s to 398 K and then holding the sample at 398 K for 20 mins to complete the desorption of water [again, we did not heat the sample above 398 K to prevent decomposition of the HKUST-1 film]. It is the same heating process used for the activation of our HKUST-1 thin films in this study. The H_2O desorption shown in Figure 5a and Figure 5b first displays a desorption peak at 190 K, which starts from 150 K. This peak is due to the multilayers of H_2O on the HKUST-1 surface and is characterized by the H_2O signal intensity increasing sharply from ~ 150 K and then rapidly dropping right after 190 K. This desorption behavior is similar to the zeroth order desorption by multilayers of H_2O molecules on metal and metal oxide surfaces as previously studied.[117,118] Although the H_2O molecules continuously desorb until 270 K, the desorption behavior is slightly changed after finishing the multilayer H_2O desorption at 190 K, which could involve another desorption feature. Moreover, the sample holder itself, which is made of tantalum (Ta), shows multilayer H_2O desorption at ~ 190 K (black line in Figure 5a), but its intensity quickly drops above 190 K, and also has a lower intensity compared to the 5 cycled HKUST-1, which is indicated in the inset of Figure 5a and Figure S8. Thus, we also tested the adsorption of H_2O at 200 K with the same H_2O pressure and exposure time as with the 120 K experiments to avoid the formation of H_2O multilayers. Water adsorption at 200 K will not create a multilayer so no desorption feature for multilayer water is expected.

During the desorption test of H_2O adsorbed on the 5 cycled HKUST-1 film at 200 K, there is a new broad desorption peak at ~ 240 K. Its desorption range (200 K to 270 K) corresponds to the temperature range in which the desorption behavior of H_2O adsorbed at 120 K was changed. The H_2O molecules desorbing in this temperature range could be molecularly adsorbed H_2O molecules near the MOF-vacuum interface.[119] If we assume that these H_2O molecules desorb from the near surface, a Redhead analysis can be adopted to estimate the desorption energy of the H_2O,[120] and this analysis yields a value of ~ 60 kJ/mol. This value is close to previously measured H_2O adsorption energies for HKUST-1 (48 - 55 kJ/mol).[110–113] As shown in Figure S8, chemisorbed H_2O molecules on our Ta sample holder desorb from 215 K to 290 K when the Ta sample holder is solely exposed to H_2O at 200 K. Although this temperature range is a little bit higher than the low temperature H_2O desorption feature observed in the HKUST-1 sample, it could contribute to the H_2O desorption from the 5 cycled HKUST-1 film. However, we have already observed in the H_2O adsorption tests at 120 K that the 5 cycled HKUST-1 film shows more H_2O desorption above 190 K compared to the Ta sample holder. Furthermore, the top surface of the sample holder was covered by a HKUST-1 thin film sample during the H_2O adsorption and desorption tests of the HKUST-1 thin film. Thus the H_2O generation during the TPD of the HKUST-1 thin film can be mainly attributed to the HKUST-1 structures. When adsorption of H_2O is conducted at 240 K, the relatively small desorption feature between 200 and 270 K disappears as indicated in Figure 5 (blue traces).

In all the H_2O desorption tests, with H_2O molecules adsorbed at 120 K, 200 K, and 240 K, the remaining strongly chemisorbed H_2O molecules begin to desorb from ~ 320 K and continue the desorption through 398 K. In particular, most of the H_2O desorption occurs while the sample is held at 398 K, which is further evidence for the gas capture capability of our HKUST-1 thin films, since the Ta sample holder itself does not show any H_2O desorption features above 190 K. This H_2O desorption temperature range is similar to the previous TGA analysis of HKUST-1,[78,116] which shows a rapid weight loss from 25 °C (298 K) to 150 °C (423 K) by water and other solvents. The number of adsorbed H_2O molecules is also controllable based on the H_2O exposure time as shown in Figure 5c for an adsorption temperature of 200 K. Here we arbitrarily define the relative quantity of desorbing H_2O molecules for the 30 minute H_2O exposure case as 1.0. With decreasing H_2O exposure time from 30 mins to 4 mins, the quantity of desorbing H_2O molecules linearly decreases, with a R^2 value of 0.99. After these H_2O adsorption and desorption tests, GAXRD of the HKUST-1 film

Please do not adjust margins

showed the same XRD diffraction patterns as the fresh sample (shown in Figure S9). These results indicate that our HKUST-1 thin films grown under vacuum also have the capability to repeatably capture gas molecules in their pores similar to HKUST-1 powder samples. Our results demonstrate that TPD is an effective experimental method for analyzing the desorption behavior of strongly adsorbed gas molecules on MOFs under vacuum at various temperatures, some of which may be difficult to be detected in conventional isotherm experiments.

Conclusions

We developed a new solvent-free HKUST-1 thin film growth method employed under vacuum by adopting a LBL deposition strategy involving the sequential physical vapor deposition of Cu followed by chemical vapor deposition of H_3BTC. After back-filling O_2 and H_2O gases up to 5.0 x 10^{-5} Torr, we initially deposited 4 ML of Cu (~ 1 nm) on a SiO_2/Si(100) substrate and then exposed H_3BTC and Cu in turn using layer-by-layer (LBL) growth. The H_3BTC source evaporator was held at 200 °C during the growth, and we fixed the amount of evaporation time of H_3BTC in each cycle at 3 mins. Based on this fixed amount of H_3BTC, we optimized the amount of Cu in each cycle by growing 5 cycled samples and measuring XPS to verify the oxidation state of Cu. As determined by XPS, 1 ML Cu deposition after each H_3BTC deposition cycle showed the best Cu^{2+} to Cu^{1+}/Cu^0 ratio compared to other tested amounts of Cu (0.5 ML and 1.5 ML) in our experimental setup, and there was no trace of copper oxide formation. We also found that the unannealed 5 cycles of H_3BTC formed supramolecular structures which exhibited similar XRD patterns to the 5 cycles of the HKUST-1 film. However, after annealing the 5 cycled H_3BTC at 343 K for 15 mins, which is the same annealing process to finalize the growth of our HKUST-1 films, they no longer showed crystallinity and became randomly ordered. This suggests that the HKUST-1 thin film structures are derived from the 3D supramolecular structures of H_3BTC molecules, and deposited Cu atoms work as joints for the H_3BTC ligand to keep their HKUST-1 like structure. For investigating the effect of background gases of O_2 and H_2O during HKUST-1 growth, we grew several 5 cycled HKUST-1 films with different background gas conditions and discovered that H_2O molecules clearly enhance the conversion of Cu^0 to Cu^{2+} in the HKUST-1 film deposition. In the analysis of the crystallinity of the HKUST-1 thin films, the (220) and (222) planes were determined to be dominant planes in the GAXRD and IPXRD measurements respectively, which shows that our HKUST-1 thin films are highly oriented. Furthermore, the thickness of HKUST-1 thin films increased linearly depending on the number of LBL cycles, ~ 20 nm for each LBL cycle as verified by AFM. We also conducted H_2O adsorption and desorption tests on a 5 cycled HKUST-1 film, which has a thickness of ~ 100 nm. The H_2O adsorption was conducted at 120 K, 200 K, and 240 K by back-filling the vacuum chamber with 2.0 x 10^{-6} Torr of H_2O for 30 mins. The H_2O desorption measured by QMS showed that most of the H_2O desorption occurred when the sample was isothermally heated at 398 K (125 °C). These results correspond to previous TGA measurements on HKUST-1 and indicate that these constant pressure H_2O adsorption and desorption tests under vacuum are able to detect strongly bound H_2O molecules in HKUST-1. Therefore, this study suggests that HKUST-1 thin films can be grown under vacuum without the use of any solvents, where its thickness is also controllable within ~ 20 nm scale. We expect this vacuum based MOF growth can be applied in various fields such as semiconductors, sensors and membranes.

Acknowledgements

We are thankful for the generous support of the Army Research Office via contract number W911NF1710214, a 9 month grant through their Short-Term Innovative Research (STIR) Program which allowed us to begin this project and also the Department of Energy Basic Energy Sciences (Grant DE-SC0018116) and Welch Foundation (Grant F-1436 (CBM) and Grant F-1929 (BKK)) which allowed us to complete the project. S. Han acknowledges the Dorothy Banks Fellowship for partial support.

Notes and references

1 D. Zhao, D. J. Timmons, D. Yuan and H.-C. Zhou, *Acc. Chem. Res.*, 2011, **44**, 123–33.

2 D. J. Tranchemontagne, J. L. Mendoza-Cortés, M. O'Keeffe and O. M. Yaghi, *Chem. Soc. Rev.*, 2009, **38**, 1257–83.

3 M. P. Suh, H. J. Park, T. K. Prasad and D.-W. Lim, *Chem. Rev.*, 2012, **112**, 782–835.

4 N. L. Rosi, J. Eckert, M. Eddaoudi, D. T. Vodak, J. Kim, M. O'Keeffe and O. M. Yaghi, *Science*, 2003, **300**, 1127–9.

5 Z. Guo, H. Wu, G. Srinivas, Y. Zhou, S. Xiang, Z. Chen, Y. Yang, W. Zhou, M. O'Keeffe and B. Chen *Angew. Chem. Int. Ed.*, 2011, **50**, 3178–3181.

6 S. Ma, D. Sun, J. M. Simmons, C. D. Collier, D. Yuan and H.-C. Zhou, *J. Am. Chem. Soc.*, 2008, **130**, 1012–6.

7 W. Zhou, H. Wu and T. Yildirim, *J. Am. Chem. Soc.*, 2008, **130**, 15268–9.

8 H. Montes-Andrés, G. Orcajo, C. Mellot-Draznieks, C. Martos, J. A. Botas and G. Calleja, *J. Phys. Chem. C*, 2018, **122**, 28123–28132.

9 K. V. Kumar, K. Preuss, M. M. Titirici and F. Rodríguez-Reinoso, *Chem. Rev.*, 2017, **117**, 1796–1825.

10 A. O. Yazaydın, R. Q. Snurr, T.-H. Park, K. Koh, J. Liu, M. D. LeVan, A. I. Benin, P. Jakubczak, M. Lanuza, D. B. Galloway, J. J. Low and R. R. Willis, *J. Am. Chem. Soc.*, 2009, **131**, 18198–18199.

11 K. Sumida, D. L. Rogow, J. a Mason, T. M. McDonald, E. D. Bloch, Z. R. Herm, T.-H. Bae and J. R. Long, *Chem. Rev.*, 2012, **112**, 724–81.

12 W. R. Lee, S. Y. Hwang, D. W. Ryu, K. S. Lim, S. S. Han, D. Moon, J. Choi and C. S. Hong, *Energy Environ. Sci.*, 2014, **7**, 744–751.

13 M. Ding, R. W. Flaig, H.-L. Jiang and O. M. Yaghi, *Chem. Soc. Rev.*, 2019, **48**, 2783–2828.

14 P. M. Bhatt, Y. Belmabkhout, A. Cadiau, K. Adil, O. Shekhah,

This journal is © The Royal Society of Chemistry 20xx

Please do not adjust margins

A. Shkurenko, L. J. Barbour and M. Eddaoudi, *J. Am. Chem. Soc.*, 2016, **138**, 9301–9307.
15 Z. R. Herm, B. M. Wiers, J. a Mason, J. M. van Baten, M. R. Hudson, P. Zajdel, C. M. Brown, N. Masciocchi, R. Krishna and J. R. Long, *Science*, 2013, **340**, 960–4.
16 E. D. Bloch, W. L. Queen, R. Krishna, J. M. Zadrozny, C. M. Brown and J. R. Long, *Science*, 2012, **335**, 1606–1610.
17 Y.-S. Bae, C. Y. Lee, K. C. Kim, O. K. Farha, P. Nickias, J. T. Hupp, S. T. Nguyen and R. Q. Snurr, *Angew. Chem. Int. Ed.*, 2012, **51**, 1857–1860.
18 H. Wang, X. Dong, J. Lin, S. J. Teat, S. Jensen, J. Cure, E. V. Alexandrov, Q. Xia, K. Tan, Q. Wang, D. H. Olson, D. M. Proserpio, Y. J. Chabal, T. Thonhauser, J. Sun, Y. Han and J. Li, *Nat. Commun.*, 2018, **9**, 1–11.
19 D.-X. Xue, Y. Belmabkhout, O. Shekhah, H. Jiang, K. Adil, A. J. Cairns and M. Eddaoudi, *J. Am. Chem. Soc.*, 2015, **137**, 5034–5040.
20 Q. Guo, L. Ren, P. Kumar, V. J. Cybulskis, K. A. Mkhoyan, M. E. Davis and M. Tsapatsis, *Angew. Chem. Int. Ed.*, 2018, **57**, 4926–4930.
21 M. H. Sun, S. Z. Huang, L. H. Chen, Y. Li, X. Y. Yang, Z. Y. Yuan and B. L. Su, *Chem. Soc. Rev.*, 2016, **45**, 3479–3563.
22 K. Otake, Y. Cui, C. T. Buru, Z. Li, J. T. Hupp and O. K. Farha, *J. Am. Chem. Soc.*, 2018, **140**, 8652–8656.
23 K. Shen, X. Chen, J. Chen and Y. Li, *ACS Catal.*, 2016, **6**, 5887–5903.
24 S. M. J. Rogge, A. Bavykina, J. Hajek, H. Garcia, A. I. Olivos-Suarez, A. Sepúlveda-Escribano, A. Vimont, G. Clet, P. Bazin, F. Kapteijn, M. Daturi, E. V. Ramos-Fernandez, F. X. Llabrés i Xamena, V. Van Speybroeck and J. Gascon, *Chem. Soc. Rev.*, 2017, **46**, 3134–3184.
25 S. Han, H. Kim, J. Kim and Y. Jung, *Phys. Chem. Chem. Phys.*, 2015, **17**, 16977–16982.
26 M. Kurmoo, *Chem. Soc. Rev.*, 2009, **38**, 1353–79.
27 P. Dechambenoit and J. R. Long, *Chem. Soc. Rev.*, 2011, **40**, 3249–65.
28 G. J. Halder, *Science*, 2002, **298**, 1762–1765.
29 J. Liu and C. Wöll, *Chem. Soc. Rev.*, 2017, **46**, 5730–5770.
30 G. Lu and J. T. Hupp, *J. Am. Chem. Soc.*, 2010, **132**, 7832–7833.
31 I. Stassen, B. Bueken, H. Reinsch, J. F. M. Oudenhoven, D. Wouters, J. Hajek, V. Van Speybroeck, N. Stock, P. M. Vereecken, R. Van Schaijk, D. De Vos and R. Ameloot, *Chem. Sci.*, 2016, **7**, 5827–5832.
32 A. L. Robinson, V. Stavila, T. R. Zeitler, M. I. White, S. M. Thornberg, J. A. Greathouse and M. D. Allendorf, *Anal. Chem.*, 2012, **84**, 7043–7051.
33 K. J. Erickson, F. Léonard, V. Stavila, M. E. Foster, C. D. Spataru, R. E. Jones, B. M. Foley, P. E. Hopkins, M. D. Allendorf and A. A. Talin, *Adv. Mater.*, 2015, **27**, 3453–3459.
34 A. A. Talin, A. Centrone, A. C. Ford, M. E. Foster, V. Stavila, P. Haney, R. A. Kinney, V. Szalai, F. El Gabaly, H. P. Yoon, F. Léonard and M. D. Allendorf, *Science*, 2014, **343**, 66–69.
35 V. Stavila, A. A. Talin and M. D. Allendorf, *Chem. Soc. Rev.*, 2014, **43**, 5994–6010.
36 F. Ke, Y.-P. Yuan, L.-G. Qiu, Y.-H. Shen, A.-J. Xie, J.-F. Zhu, X.-Y. Tian and L.-D. Zhang, *J. Mater. Chem.*, 2011, **21**, 3843.
37 K. Ariga, Y. M. Lvov, K. Kawakami, Q. Ji and J. P. Hill, *Adv. Drug Deliv. Rev.*, 2011, **63**, 762–771.
38 M. Shete, P. Kumar, J. E. Bachman, X. Ma, Z. P. Smith, W. Xu, K. A. Mkhoyan, J. R. Long and M. Tsapatsis, *J. Memb. Sci.*, 2018, **549**, 312–320.
39 R. Ranjan and M. Tsapatsis, *Chem. Mater.*, 2009, **21**, 4920–4924.
40 X. Ma, P. Kumar, N. Mittal, A. Khlyustova, P. Daoutidis, K. A. Mkhoyan and M. Tsapatsis, *Science*, 2018, **361**, 1008–1011.
41 J. Liu and C. Wöll, *Chem. Soc. Rev.*, 2017, **46**, 5730–5770.
42 V. Chernikova, O. Shekhah and M. Eddaoudi, *ACS Appl. Mater. Interfaces*, 2016, **8**, 20459–20464.
43 C. Sapsanis, H. Omran, V. Chernikova, O. Shekhah, Y. Belmabkhout, U. Buttner, M. Eddaoudi and K. Salama, *Sensors*, 2015, **15**, 18153–18166.
44 V. Chernikova, O. Yassine, O. Shekhah, M. Eddaoudi and K. N. Salama, *J. Mater. Chem. A*, 2018, **6**, 5550–5554.
45 A. Bouchaala, N. Jaber, O. Yassine, O. Shekhah, V. Chernikova, M. Eddaoudi and M. Younis, *Sensors*, 2016, **16**, 758.
46 I. Stassen, M. Styles, G. Grenci, H. Van Gorp, W. Vanderlinden, S. De Feyter, P. Falcaro, D. De Vos, P. Vereecken and R. Ameloot, *Nat. Mater.*, 2016, **15**, 304–310.
47 I. Stassen, D. De Vos and R. Ameloot, *Chem. Eur. J.*, 2016, **22**, 14452–14460.
48 S. S.-Y. Chui, *Science*, 1999, **283**, 1148–1150.
49 C. H. Hendon and A. Walsh, *Chem. Sci.*, 2015, **6**, 3674–3683.
50 J. Liu, Y. Wang, A. I. Benin, P. Jakubczak, R. R. Willis and M. D. LeVan, *Langmuir*, 2010, **26**, 14301–14307.
51 Q. Min Wang, D. Shen, M. Bülow, M. Ling Lau, S. Deng, F. R. Fitch, N. O. Lemcoff and J. Semanscin, *Microporous Mesoporous Mater.*, 2002, **55**, 217–230.
52 Q. Yang and C. Zhong, *ChemPhysChem*, 2006, **7**, 1417–1421.
53 A. G. Wong-Foy, A. J. Matzger and O. M. Yaghi, *J. Am. Chem. Soc.*, 2006, **128**, 3494–5.
54 H. Wu, J. M. Simmons, Y. Liu, C. M. Brown, X.-S. Wang, S. Ma, V. K. Peterson, P. D. Southon, C. J. Kepert, H.-C. Zhou, T. Yildirim and W. Zhou, *Chem. Eur. J.*, 2010, **16**, 5205–5214.
55 L. Alaerts, E. Séguin, H. Poelman, F. Thibault-Starzyk, P. A. Jacobs and D. E. De Vos, *Chem. Eur. J.*, 2006, **12**, 7353–7363.
56 N. C. Jeong, B. Samanta, C. Y. Lee, O. K. Farha and J. T. Hupp, *J. Am. Chem. Soc.*, 2012, **134**, 51–54.
57 E. Biemmi, C. Scherb and T. Bein, *J. Am. Chem. Soc.*, 2007, **129**, 8054–8055.
58 O. Shekhah, H. Wang, S. Kowarik, F. Schreiber, M. Paulus, M. Tolan, C. Sternemann, F. Evers, D. Zacher, R. A. Fischer and C. Wöll, *J. Am. Chem. Soc.*, 2007, **129**, 15118–15119.
59 D. Zacher, A. Baunemann, S. Hermes and R. A. Fischer, *J. Mater. Chem.*, 2007, **17**, 2785.
60 B. K. Keitz, C. J. Yu, J. R. Long and R. Ameloot, *Angew. Chem. Int. Ed.*, 2014, **53**, 5561–5565.

Please do not adjust margins

61 Y. Guo, Y. Mao, P. Hu, Y. Ying and X. Peng, *ChemistrySelect*, 2016, **1**, 108–113.
62 P. C. Lemaire, J. Zhao, P. S. Williams, H. J. Walls, S. D. Shepherd, M. D. Losego, G. W. Peterson and G. N. Parsons, *ACS Appl. Mater. Interfaces*, 2016, **8**, 9514–9522.
63 S. Fabris, S. Stepanow, N. Lin, P. Gambardella, A. Dmitriev, J. Honolka, S. Baroni and K. Kern, *Nano Lett.*, 2011, **11**, 5414–5420.
64 D. Sheberla, L. Sun, M. A. Blood-Forsythe, S. Er, C. R. Wade, C. K. Brozek, A. Aspuru-Guzik and M. Dincă, *J. Am. Chem. Soc.*, 2014, **136**, 8859–8862.
65 R. Sakamoto, K. Takada, T. Pal, H. Maeda, T. Kambe and H. Nishihara, *Chem. Commun.*, 2017, **53**, 5781–5801.
66 G. Sheerin and A. A. Cafolla, *Surf. Sci.*, 2005, **577**, 211–219.
67 S. V Kolotuchin, E. E. Fenlon, S. R. Wilson, C. J. Loweth and S. C. Zimmerman, *Angew. Chem. Int. Ed.*, 1996, **34**, 2654–2657.
68 T. Classen, M. Lingenfelder, Y. Wang, R. Chopra, C. Virojanadara, U. Starke, G. Costantini, G. Fratesi, S. Fabris, S. de Gironcoli, S. Baroni, S. Haq, R. Raval and K. Kern, *J. Phys. Chem. A*, 2007, **111**, 12589–12603.
69 S. V. Kolotuchin, P. A. Thiessen, E. E. Fenlon, S. R. Wilson, C. J. Loweth and S. C. Zimmerman, *Chem. Eur. J.*, 1999, **5**, 2537–2547.
70 K. G. Nath, O. Ivasenko, J. A. Miwa, H. Dang, J. D. Wuest, A. Nanci, D. F. Perepichka and F. Rosei, *J. Am. Chem. Soc.*, 2006, **128**, 4212–4213.
71 M. Lackinger, S. Griessl, L. Kampschulte, F. Jamitzky and W. M. Heckl, *Small*, 2005, **1**, 532–539.
72 I. Cebula, H. Lu, M. Zharnikov and M. Buck, *Chem. Sci.*, 2013, **4**, 4455.
73 S. Griessl, M. Lackinger, M. Edelwirth, M. Hietschold and W. M. Heckl, *Single Mol.*, 2002, **3**, 25–31.
74 P. Messina, A. Dmitriev, N. Lin, H. Spillmann, M. Abel, J. V. Barth and K. Kern, *J. Am. Chem. Soc.*, 2002, **124**, 14000–14001.
75 K. Y. Jee, J. S. Kim, J. Kim and Y. T. Lee, *Desalin. Water Treat.*, 2016, **57**, 17637–17645.
76 B. Peng, C. Feng, S. Liu and R. Zhang, *Catal. Today*, 2018, **314**, 122–128.
77 H. Chen, L. Wang, J. Yang and R. T. Yang, *J. Phys. Chem. C*, 2013, **117**, 7565–7576.
78 Y. Wang, Y. Lü, W. Zhan, Z. Xie, Q. Kuang and L. Zheng, *J. Mater. Chem. A*, 2015, **3**, 12796–12803.
79 H. Niu, S. Liu, Y. Cai, F. Wu and X. Zhao, *Microporous Mesoporous Mater.*, 2016, **219**, 48–53.
80 A. S. Hall, A. Kondo, K. Maeda and T. E. Mallouk, *J. Am. Chem. Soc.*, 2013, **135**, 16276–16279.
81 O. Shekhah, J. Liu, R. A. Fischer and C. Wöll, *Chem. Soc. Rev.*, 2011, **40**, 1081.
82 B. Di Credico, M. Redaelli, M. Bellardita, M. Calamante, C. Cepek, E. Cobani, M. D'Arienzo, C. Evangelisti, M. Marelli, M. Moret, L. Palmisano and R. Scotti, *Catalysts*, 2018, **8**, 353.
83 P. Jiang, D. Prendergast, F. Borondics, S. Porsgaard, L. Giovanetti, E. Pach, J. Newberg, H. Bluhm, F. Besenbacher and M. Salmeron, *J. Chem. Phys.*, 2013, **138**, 024704.
84 Z. Dan, Y. Yang, F. Qin, H. Wang and H. Chang, *Materials (Basel).*, 2018, **11**, 446.
85 J. Als-Nielsen, D. Jacquemain, K. Kjaer, F. Leveiller, M. Lahav and L. Leiserowitz, *Phys. Rep.*, 1994, **246**, 251–313.
86 K. Inaba, S. Kobayashi, K. Uehara, A. Okada, S. L. Reddy and T. Endo, *Adv. Mater. Phys. Chem.*, 2013, **03**, 72–89.
87 M. Bouroushian and T. Kosanovic, *Cryst. Struct. Theory Appl.*, 2012, **01**, 35–39.
88 I. Cebula, C. Shen and M. Buck, *Angew. Chem. Int. Ed.*, 2010, **49**, 6220–6223.
89 L. Kanninen, N. Jokinen, H. Ali-Löytty, P. Jussila, K. Lahtonen, M. Hirsimäki, M. Valden, M. Kuzmin, R. Pärna and E. Nõmmiste, *Surf. Sci.*, 2011, **605**, 1968–1978.
90 A. Dmitriev, N. Lin, J. Weckesser, J. V. Barth and K. Kern, *J. Phys. Chem. B*, 2002, **106**, 6907–6912.
91 G. Xie, M. Forslund and J. Pan, *ACS Appl. Mater. Interfaces*, 2014, **6**, 7444–7455.
92 G. P. López, D. G. Castner and B. D. Ratner, *Surf. Interface Anal.*, 1991, **17**, 267–272.
93 E. Cano, J. M. Bastidas, J. L. Polo and N. Mora, *J. Electrochem. Soc.*, 2001, **148**, B431.
94 S. Y. Lu, M. Jin, Y. Zhang, Y. B. Niu, J. C. Gao and C. M. Li, *Adv. Energy Mater.*, 2018, **8**, 1–9.
95 S.-Y. Kim, A.-R. Kim, J. W. Yoon, H.-J. Kim and Y.-S. Bae, *Chem. Eng. J.*, 2018, **335**, 94–100.
96 H.-W. Tien, Y.-L. Huang, S.-Y. Yang, J.-Y. Wang and C.-C. M. Ma, *Carbon N. Y.*, 2011, **49**, 1550–1560.
97 Z. L. Xu, B. Zhang, S. Abouali, M. Akbari Garakani, J. Huang, J. Q. Huang, E. Kamali Heidari and J. K. Kim, *J. Mater. Chem. A*, 2014, **2**, 17944–17951.
98 K. Müller, J. S. Malhi, J. Wohlgemuth, R. A. Fischer, C. Wöll, H. Gliemann and L. Heinke, *Dalt. Trans.*, 2018, 16474–16479.
99 S. Amirjalayer, M. Tafipolsky and R. Schmid, *J. Phys. Chem. Lett.*, 2014, **5**, 3206–3210.
100 M. K. Bhunia, J. T. Hughes, J. C. Fettinger and A. Navrotsky, *Langmuir*, 2013, **29**, 8140–8145.
101 H. Li, M. Eddaoudi, M. O'Keeffe and O. M. Yaghi, *Nature*, 1999, **402**, 276–279.
102 A. Umemura, S. Diring, S. Furukawa, H. Uehara, T. Tsuruoka and S. Kitagawa, *J. Am. Chem. Soc.*, 2011, **133**, 15506–15513.
103 V. Marghussian, in *Nano-Glass Ceramics*, ed. V. B. T.-N.-G. C. Marghussian, Elsevier, Oxford, 2015, pp. 1–62.
104 Pallab Bhattacharya, *Semiconductor optoelectronic devices*, Prentice Hall, 2nd edn., 1997.
105 H. S. Kang, J. S. Kang, J. W. Kim and S. Y. Lee, *J. Appl. Phys.*, 2004, **95**, 1246–1250.
106 M.-S. Yao, X.-J. Lv, Z.-H. Fu, W.-H. Li, W.-H. Deng, G.-D. Wu and G. Xu, *Angew. Chem. Int. Ed.*, 2017, **56**, 16510–16514.
107 J. J. Gutiérrez-Sevillano, J. M. Vicent-Luna, D. Dubbeldam and S. Calero, *J. Phys. Chem. C*, 2013, **117**, 11357–11366.
108 J. J. Gutiérrez-Sevillano, S. Calero and R. Krishna, *J. Phys. Chem. C*, 2015, **119**, 3658–3666.
109 J. M. Castillo, T. J. H. Vlugt and S. Calero, *J. Phys. Chem. C*, 2008, **112**, 15934–15939.
110 S. K. Henninger, F. P. Schmidt and H.-M. Henning, *Appl.*

 This journal is © The Royal Society of Chemistry 20xx

Please do not adjust margins

Therm. Eng., 2010, **30**, 1692–1702.
111 L. Grajciar, O. Bludský and P. Nachtigall, *J. Phys. Chem. Lett.*, 2010, **1**, 3354–3359.
112 N. Al-Janabi, P. Hill, L. Torrente-Murciano, A. Garforth, P. Gorgojo, F. Siperstein and X. Fan, *Chem. Eng. J.*, 2015, **281**, 669–677.
113 J. R. Álvarez, E. Sánchez-González, E. Pérez, E. Schneider-Revueltas, A. Martínez, A. Tejeda-Cruz, A. Islas-Jácome, E. González-Zamora and I. A. Ibarra, *Dalt. Trans.*, 2017, **46**, 9192–9200.
114 T. R. C. Van Assche, T. Duerinck, J. J. Gutiérrez Sevillano, S. Calero, G. V. Baron and J. F. M. Denayer, *J. Phys. Chem. C*, 2013, **117**, 18100–18111.
115 P. Küsgens, M. Rose, I. Senkovska, H. Fröde, A. Henschel, S. Siegle and S. Kaskel, *Microporous Mesoporous Mater.*, 2009, **120**, 325–330.
116 E. Biemmi, A. Darga, N. Stock and T. Bein, *Microporous Mesoporous Mater.*, 2008, **114**, 380–386.
117 A. Hodgson and S. Haq, *Surf. Sci. Rep.*, 2009, **64**, 381–451.
118 S. M. McClure, D. J. Safarik, T. M. Truskett and C. B. Mullins, *J. Phys. Chem. B*, 2006, **110**, 11033–11036.
119 C. H. Sharp, J. Abelard, A. M. Plonka, W. Guo, C. L. Hill and J. R. Morris, *J. Phys. Chem. C*, 2017, **121**, 8902–8906.
120 P. A. Redhead, *Vacuum*, 1962, **12**, 203–211.

TOC

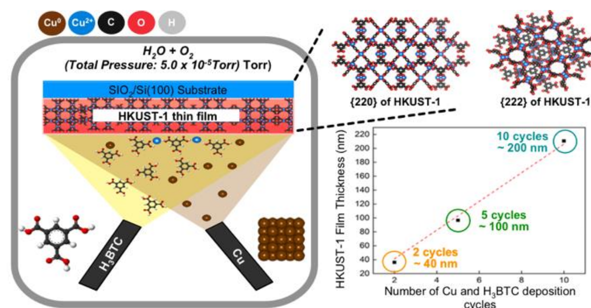

H_3BTC and Cu are sequentially deposited to form highly oriented HKUST-1 thin films under vacuum without the use of solvents.

Please do not adjust margins